Journal of Cluster Science (2023) 34:1547–1562
https://doi.org/10.1007/s10876-022-02335-1

ORIGINAL PAPER

Nanocluster of Aluminum Lattice via Organic Inhibitors Coating: A Study of Freundlich Adsorption

Fatemeh Mollaamin[1] · Sara Shahriari[2] · Majid Monajjemi[3] · Zahra Khalaj[4]

Received: 13 May 2022 / Accepted: 10 July 2022 / Published online: 29 July 2022

Abstract

The adsorption analysis of some organic inhibitors consisting of Pyridine, 2-Methylpyridine, 3-Methylpyridine, 4-Methylpyridine and 2, 4-Dimethylpyridine onto aluminum (111) metal surface based on optimized coordination of binding on the Al (111) metal surface has been accomplished. In this research, the ONIOM approach has been performed with a three-layered level of high level of DFT method using 6–31 + G* and LANL2DZ basis sets by the physico-chemical software of Gaussian 09, a medium semi-active part that includes important electronic contributions, and a low level part that has been handled using MM2 force field approaches. The physico-chemical properties of adsorption -surface complexes are one of the principal parameters for determining and choosing the adsorption. The characteristic of the metal (111)-lattice in solutions of hydrochloric acid and nitric acid by some heterocyclic compounds including Pyridine, 2-Methylpyridine, 3-Methylpyridine, 4-Methylpyridine and 2, 4-Dimethylpyridine has been estimated through NMR and IR results. Nitrogen atom in pyridine cycle with the most influence on the NMR shielding of isotropic and anisotropic tensors has leaded us toward the active site for adsorption onto Al (111) surface. Moreover, the IR spectrum for each of these heterocyclic compounds consisting of Pyridine, 2-Methylpyridine, 3-Methylpyridine, 4-Methylpyridine and 2, 4-Dimethylpyridine has been indicted in the frequency range between 500 cm^{-1} and 3250 cm^{-1} by the strongest peaks about 550 cm^{-1}, 1500 cm^{-1}, and 3250 cm^{-1}. In this work, the co-adsorption of Cl^- / $NO3^-$ anions with H^+_{ads} cation onto aluminum-surface through the optimized adsorption energy for these compounds on a top site of metal (111) has been accomplished. Our calculations have illustrated that the adsorption stability energy of pyridine and its derivatives depends on the structure, the adsorption site and the acidic media.

Keywords Langmuir adsorption · Freundlich adsorption · Metal (111) surface · DFT · NMR · IR

Introduction

It is well known that heterocyclic compounds containing nitrogen atoms are good corrosion inhibitors for many metals in various acidic media [1–11]. For example, benzotriazole on the Cu and Fe electrode [12–15], isoquinoline derivative [16] and imidazole derivatives [17] on the Fe electrode are sufficient inhibitors for corrosion of these metals [1–17]. Commonly, metal alloys are applied in the fields of automobile manufacturing, national defense industry, aviation industry, electronics and daily important manufacturing with their perfect properties [18]. In fact, aluminum is produced by Hall-Héroult method with problems of high energy consumption, serious corrosion of equipment, environmental pollution etc. [19, 20]. It is necessary to explore a low-temperature green production method of metal, and it is also a research turning point in this field. Recently, a magnificent development has been seen in low temperature metal electrolysis. It has been focused on the replacement of cryolite molten salt system by molten salt system with lower melting point such as chloride or fluoride. These methods can reduce the electrolysis temperature to a certain extent, but the reduction is not enough [18–20]. The appearance of

✉ Fatemeh Mollaamin
smollaamin@gmail.com

[1] Department of Biomedical Engineering, Faculty of Engineering and Architecture, Kastamonu University, Kastamonu, Turkey

[2] Department of Chemistry, Central Tehran Branch, Islamic Azad University, Tehran, Iran

[3] Department of Chemical Engineering, Central Tehran Branch, Islamic Azad University, Tehran, Iran

[4] Department of Physics, Shahr-E-Qods Branch, Islamic Azad University, Tehran, Iran

ionic liquids provides a possibility for the development of low-temperature aluminum electrolysis technology.

In some studies, an ionic system has been discovered composing of some inorganic or organic anions and organic cations and is liquid at or near room temperature [21–24]. It has the advantages of non-volatile, wide electrochemical window, wide liquid temperature range, good thermal stability, conductivity and variable combination of properties, and is largely applied in different fields such as electrochemistry, catalysis, organic synthesis, extraction and separation [21–32].

In recent years, ionic liquids, as a new type of green electrolyte, have been used for aluminum electro-deposition and electrolysis refining at or near room temperature and some development has been made [26–31]. Nevertheless, there are still some problems to be solved, such as high electrolyte viscosity and dendrite phenomenon in the deposition layer [27–30]. The addition of additives is one of the common methods to address these problems [31, 32].

In recent years, some progress has been made through the impacts of additives such as chloride, acetonitrile, aromatic compounds, carbonyl small molecules, halo-alkanes, nicotinic acid and their derivatives on electro-deposition of aluminum in ionic liquids [33–36].

The influence of methyl carbonate on electro-deposition of metal in [EMIM] $Cl/AlCl_3$ system by cyclic voltammetry was accomplished [37]. It has been explored that that Nano Al could be prepared by adding nicotinic acid into [EMIM] $Cl/AlCl_3$ [38, 39].

When various properties of organic compounds are to be expressed, it is necessary that the electron structure of a set of organic compounds be studied. Organic substances utilized as corrosion inhibitors were selected and judged on the basis of their physicochemical properties [40, 41], and relatively little attention has been paid to the quantitative evaluation of the internal and steric effect of these substances upon their inhibition efficiency. Although a lot about inhibition of corrosion by aniline derivatives has been investigated, the series of p-substituted anilines seems to be very suitable for verifying the previously obtained quantum chemical and corrosion inhibition dependencies, and also, it was interesting to study the protonated forms [42].

Recently, it has been investigated the interaction between imidazole and the Al (111)-lattice. This surface is often used in experimental investigations as it is easy to prepare and clean using standard annealing methods and sputtering techniques, making it an ideal prototype metal substrate [43]. The interaction of imidazole building blocks with metal surfaces is also of particular interest to the zeolite community as there has been a growing trend in coupling porous materials, such as zeolite imidazole frameworks (ZIFs), with metallic supports to create a new type of functional materials [44, 45]. These meta-materials are developed to improve on the current properties of ZIFs for gas separation, gas storage and catalysis [46–48].

The inhibition efficiency depends on the parameters of system: metal composition, pH and structure of inhibitor molecule. It is well known that heterocyclic compounds containing nitrogen atoms are good corrosion inhibitors for many metals in various acidic media, for example: benzotriazole at the Cu and Fe electrode, isoquinoline derivatives and imidazole derivatives at the Fe electrode are sufficient inhibitors for corrosion of these metals [49–65]. Recently, it was reported that pyridine and its derivatives had been used as corrosion inhibitors of the aluminum electrode [66, 67]. The present work is an extension of the earlier work and reports the role of Pyridine, 2-Methylpyridine, 4-Methylpyridine and 2, 4-Dimethylpyridine as corrosion inhibitors for aluminum surface in hydrochloric acid (HCl) and nitric acid (HNO,). In this paper, quantum chemical values of these substances were calculated by the HF and B3LYP methods.

These days, with the development of computational techniques and methods, First Principles method has become the effective means to study the structure, properties and reaction mechanism of compounds and materials. By calculating the frontier orbital distribution, Fukui index, charge distribution of heavy atoms and other quantum chemical parameters, people can study the reaction activity, charge transfer, structure–activity relationship and so on.

The microscopic interaction and reaction mechanism between molecules can be deeply revealed from these quantum chemical parameters, which provide a useful way to understand adsorption behavior between molecules and interfaces at the atomic and molecular levels. It has been successfully applied to the study of various metal lattice properties [69–71]. Valencia et al. studied the adsorption mechanism of [EMIM]BF_4 on the Li(100) lattice with density functional theory (DFT), and found that adding a small amount of [EMIM]BF_4 to Li ion battery can prevent dendrite formation and improve battery performance [68, 69].

Clarke et al. studied the effect of [$EtNH_3$] BF_4 on the Li-ion battery system by DFT and molecular dynamics simulation (MD). These works provide a new way to explore the interaction mechanism between additives and metal lattice in ionic liquids [70]. Aromatic compounds, as a kind of ring compounds with delocalized bonds, are widely used as additives in electrolysis and electroplating because of their stable structure and difficult decomposition. Pyridine derivatives have been widely used because of their strong polarization and leveling ability in solution and ionic liquids. It is found that Nicotin-amide, Pyridine-2-formamide and Pyridine-4-formamide can be used as effective leveling agents for electro-deposition of aluminum in [Bmim] $Cl/AlCl_3$ [71]. The results showed that the order of the deposition was Nicotin-amide > Pyridine-2-formamide > Pyridine-4-formamide. However, the mechanism is still unclear, especially

the interaction between additives and electrode, charge transfer and adsorption behavior and characteristics. Due to its stable chemical properties and low hydrogen evolution over potential, platinum has a very important application in electrochemistry, such as auxiliary electrode, modified electrode substrate, electro-catalysis, etc. Platinum electrode is commonly used in the measurement of electrochemical properties of aqueous solution, molten salt, organic electrolyte and ionic liquid, such as cyclic voltammetry, polarization curve and electrochemical impedance. Therefore, it is very important to study the adsorption of molecules on the lattice of Pt electrode. At the same time, Platinum has good catalytic performance, which is used as a catalyst in fuel cell, petrochemical industry, automobile exhaust purification and other fields [72].

Material and Method

Pyridine and its Derivatives

Pyridine is a weak alkaline, water-miscible liquid with chemical formula of C_5H_5N as an organic compound with a principal heterocyclic structure which has the potential of adsorption onto surfaces for preventing and deducing degradation rates [73, 74]. 2-Methylpyridine with formula C_6H_7N is the compound colorless and liquid having unpleasant odor like pyridine that is basically employed to produce vinylpyridine and the agrichemical nitrapyrin. 2-methypyridine and 4-methypyridine are more degradable and indicate less effect during volatizing from compounds in environment than 3-methypyridine [73, 74].

A dimethyl derivative of pyridine (C_7H_9) is Dimethylpyridine with identical properties with pyridine, but the existence of the methyl groups might prevent some of the more direct activities through several isomers of 2,3-Dimethyl Pyridine; 2,4-Dimethylpyridine; 2,5-Dimethylpyridine; 2,6-Dimethylpyridine; 3,4-Dimethylpyridine; and 3,5-Dimethylpyridine [73, 74].

NMR Method

1H-NMR calculations on inhibitors of Pyridine and four derivatives of 2-Methylpyridine, 3-Methylpyridine, 4-Methylpyridine and 2, 4-Dimethylpyridine have been estimated to unravel the indicated atoms of nitrogen, carbon and hydrogen in the active sites of these compounds through the formation of the binding between inhibitors and surface (Scheme1).

The 1H- NMR measurements demonstrate the active sites of Pyridine and four derivatives of 2-Methylpyridine, 3-Methylpyridine, 4-Methylpyridine and 2, 4-Dimethylpyridine for binking to the Al (111)—surface exploring the most electronegative atoms for attaching to the Al (111)-surface which represent the maximal shift in all levels in the 1H-NMR spectra (Scheme1).

Then, the NMR data of isotropic (σ_{iso}), anisotropic shielding tensor (σ_{aniso}), and eigenvalues of chemical shielding including σ_{11}, σ_{22}, σ_{33} for Pyridine and four derivatives of 2-Methylpyridine, 3-Methylpyridine, 4-Methylpyridine and 2, 4-Dimethylpyridine have been calculated using Gaussian 09 program software [75] and reported in Table 1.

Moreover, the solution of H^+, Cl^- and NO_3^- has impacted on the nuclear magnetic resonance data and chemical shielding of nitrogen, carbon and hydrogen atoms in Pyridine and four derivatives of 2-Methylpyridine, 3-Methylpyridine, 4-Methylpyridine and 2, 4-Dimethylpyridine (Fig. 1). In Fig. 1, it has been indicated that nitrogen atom in pyridine cycle has the most influence on the NMR shielding which directs us toward the active site for adsorption onto Al (111) surface.

The quantum chemical calculations yield the CS tensors in principal axes system to evaluate the isotropic chemical-shielding (CSI), anisotropic chemical-shielding (CSA) [76]:

$$\mathrm{CSI(ppm)} = \left(\sigma_{33} + \sigma_{22} + \sigma_{11}\right)/3 \quad (1)$$

$$\mathrm{CSA(ppm)} = \sigma_{33} - \left(\sigma_{22} + \sigma_{11}\right)/2 \quad (2)$$

In fact, we have found that the isotropic and anisotropy shielding increase with the occupancy and consequently the negative charge in pyridine cycle influenced by nitrogen atom (Fig. 1).In Fig. 1, it has been exhibited that the graph of nitrogen atom has the same attitude but a considerable deviation from carbon and hydrogen atoms.

IR Method

The infrared (IR) calculations have been accomplished for Pyridine and four derivatives of 2-Methylpyridine, 3-Methylpyridine, 4-Methylpyridine and 2, 4-Dimethylpyridine at different levels of theory to obtain the more accurate equilibrium geometrical parameters, IR spectral (Scheme 2) and data for each of the determined structure. The IR spectrum for each of these compounds has been seen in the frequency range between 500 cm^{-1}–3250 cm^{-1} by the strongest peaks about 550 cm^{-1}, 1500 cm^{-1}, 3250 cm^{-1} for Pyridine, 2-Methylpyridine, 3-Methylpyridine, 4-Methylpyridine and 2, 4-Dimethylpyridine (Scheme 2).

Scheme 2 demonstrates the relationship between intensity and frequency of Pyridine and four derivatives of 2-Methylpyridine, 3-Methylpyridine, 4-Methylpyridine and 2, 4-Dimethylpyridine in different normal modes of sharp peaks at B3LYP/6–31 + G* methods. The calculations of the relative harmonic frequencies, IR intensities, dipole moments and ΔH, ΔG, ΔS for active points of Pyridine and

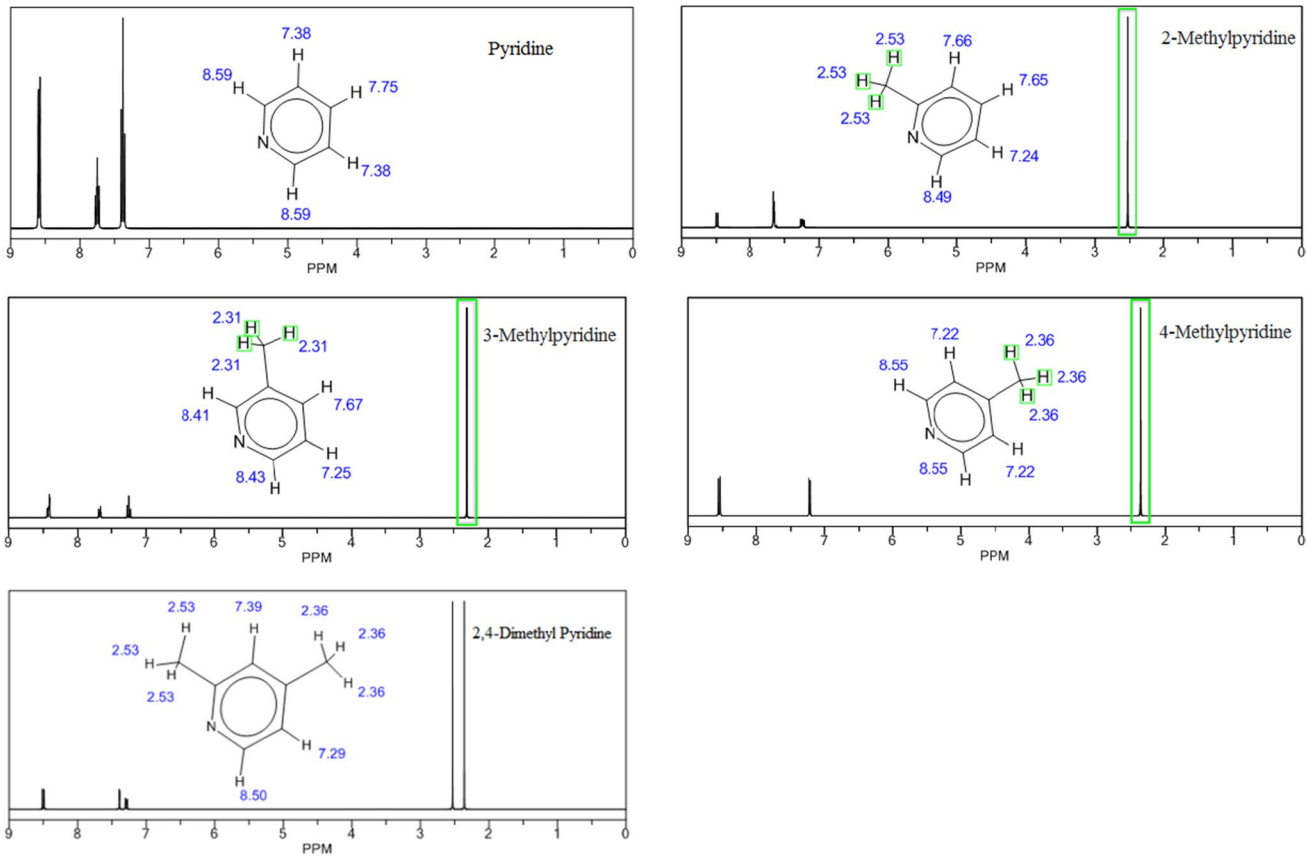

Scheme 1 1H-NMR spectra of Pyridine and four derivatives of 2-Methylpyridine, 3-Methylpyridine, 4-Methylpyridine and 2, 4-Dimethylpyridine through the adsorption process by indicating the active zone of these compounds becoming close to the Al (111)-surface

four derivatives of 2-Methylpyridine, 3-Methylpyridine, 4-Methylpyridine and 2, 4-Dimethylpyridine have been reported in Table 2.

Figure 2 has illustrated that the variation of Gibbs free energy behaves as a linear relation observed between temperature and ΔS which increases with temperature:

$$\Delta G = -T\Delta S + \Delta H \quad (3)$$

$$\Delta G = -9.8604T - 150.79; R^2 = 0.8 \quad (4)$$

ONIOM Simulation

In this work, it has been performed the advanced ONIOM simulation. So, the combination of three levels in decreasing order of accuracy has been defined including high, medium, and low levels of theory. High-level has been done using the DFT method of B3LYP with 6–31 + G* basis set for carbon and hydrogen atoms and LANL2DZ for some aluminum atoms in the adsorption cites. Medium-level has been done on the nitrogen, carbon and hydrogen in the adsorption cites due to semi-empirical methods. Finally, a low-level has been performed on the other aluminum atoms with MM2 force fields (Scheme 3) [77].

$$E_{ONIOM} = E_{high} + E_{medium} + E_{low} \quad (5)$$

The three-layered method of ONIOM permits us to investigate a larger system more precisely than the one-layered model which can treat a medium size system very accurately like a very large system with modest accuracy [78].

This three-layered model has been employed to activation barriers for the pyridine, 2-Methylpyridine, 3-Methylpyridine, 4-Methylpyridine and 2, 4-Dimethylpyridine onto aluminum (111) metal surface. In general, the results for both geometry optimizations and single point energy calculations agree well with benchmark predictions.

We have run a density functional theory (DFT) study on the mechanisms onto Al(111) up to adsorbed by N-atoms of Pyridine, 2-Methylpyridine, 3-Methylpyridine, 4-Methylpyridine and 2, 4-Dimethylpyridine. We have found that the surface binding site preferences of N-atoms are largely affected by the presence of neighboring N-atoms. The

Table 1 NMR properties of some atoms for Pyridine and four derivatives of 2-Methylpyridine, 3-Methylpyridine, 4-Methylpyridine and 2, 4-Dimethylpyridine in ppm at the adsorption site onto Al-surface

Pyridine										
ppm	N1	C2	C3	C4	C5	C6	H7	H8	H9	H10
σ_{11}	−415.8484	−55.6476	−55.6325	−26.6582	−34.2200	−26.6683	21.0956	21.0941	23.1044	22.6162
σ_{22}	−139.9757	42.9145	42.9109	69.9254	43.5949	69.9111	22.7184	22.7195	24.8441	25.2658
σ_{33}	298.5734	158.4674	158.4718	183.6880	189.4656	183.6859	27.3881	27.3886	27.9334	27.6759
σ_{iso}	−85.7502	48.5781	48.5834	75.6517	66.2801	75.6429	23.7340	23.7341	25.2940	25.1859
σ_{aniso}	576.4855	164.8340	164.8326	162.0544	184.7781	162.0645	5.4811	5.4817	3.9592	3.7349
2-Methylpyridine										
ppm	N1	C2	C3	C4	C7	H8	H9	H12	H13	H14
σ_{11}	−427.9947	−55.8361	−55.2599	−24.0264	146.6990	21.4826	22.8963	26.4033	26.4181	26.4033
σ_{22}	−124.1781	50.0577	21.7570	73.5525	165.1137	22.7184	24.2815	28.8013	30.9764	28.8013
σ_{33}	296.9953	157.6795	156.0693	173.9242	193.6457	27.4278	29.9916	35.0529	35.0395	35.0529
σ_{iso}	−85.0592	50.6337	40.8554	74.4834	168.4861	23.8763	25.7231	30.0858	30.8114	30.0858
σ_{aniso}	573.0817	160.5687	172.8207	149.1611	37.7393	5.3273	6.4027	7.4506	6.3423	7.4506
3-Methylpyridine										
ppm	N1	C2	C3	C4	C7	H8	H9	H12	H13	H14
σ_{11}	−460.6697	−50.3439	−53.5888	−30.3435	153.0595	21.5865	21.0897	25.9726	26.7095	25.9739
σ_{22}	−131.9599	51.4421	55.1546	34.0059	170.5739	22.6655	21.4032	29.1668	30.8906	29.1677
σ_{33}	305.9783	160.3759	150.6288	186.0586	195.5358	27.6310	28.9794	35.6328	35.8269	35.6338
σ_{iso}	−95.5504	53.8247	50.7315	63.2403	173.0564	23.9610	23.8241	30.2574	31.1423	30.2585
σ_{aniso}	602.2931	159.8268	149.8459	184.2273	33.7191	5.5050	7.7329	8.0631	7.0269	8.0630
4-Methylpyridine										
ppm	N1	C2	C3	C5	C7	H8	H9	H12	H13	H14
σ_{11}	−442.8446	−54.8676	−54.5144	−37.5648	150.3669	21.5589	21.4305	25.9222	26.3870	25.9222
σ_{22}	−124.1064	49.2261	49.9527	16.7197	168.1602	22.3079	22.3144	29.2645	30.7531	29.2645
σ_{33}	310.1984	157.2010	157.7865	187.2899	196.1229	27.9207	27.9080	35.7194	35.8803	35.7194
σ_{iso}	−85.5842	50.5198	51.0749	55.4816	171.5500	23.9292	23.8843	30.3021	31.0068	30.3021
σ_{aniso}	593.6738	160.0217	160.0673	197.7124	36.8594	5.9873	6.0355	8.1260	7.3102	8.1260
2, 4-Dimethylpyridine										
ppm	N1	C2	C3	C5	C7	C8	H12	H13	H15	H16
σ_{11}	−411.5838	−54.3551	−53.5042	−37.3973	146.9390	150.7271	26.4246	26.2725	25.8744	26.3501
σ_{22}	−117.0329	50.1313	22.7822	16.2475	165.2607	168.1174	28.7276	31.3274	29.4641	30.7157
σ_{33}	299.0557	154.7457	153.8136	184.3507	193.8190	196.3136	35.2331	34.9493	35.7291	36.0721
σ_{iso}	−76.5204	50.1740	41.0305	54.4003	168.6729	171.7194	30.1285	30.8497	30.3559	31.0460
σ_{aniso}	563.3641	156.8576	169.1746	194.9256	37.7191	36.8913	7.6570	6.1493	8.0598	7.5392

calculated Al-N pair distribution functions have indicated that the formation of clusters directs to shorter Al-N bond lengths when compared to the homogeneous growth.

In this research, atomic structure of the Al (111) surface has been built using Gaussian 09 program package through geometry coordination and optimized total-energy calculation. Result observations have revealed that the Al (111) surface calculated with the obtained structure parameters are in good agreement with those metal (111) achieved from other experimental calculations [79–84].

In fact, hybrid functional is a group of approximations for the exchange–correlation energy functional in DFT (Density Functional Theory) which combines a part of exact exchange from HF (Hartree–Fock theory) method with the rest of the exchange–correlation energy from other information such as empirical or ab initio methodologies. Therefore, the exact exchange energy functional is illustrated by the Kohn–Sham orbitals instead of the density, so is placed as the indirect density functional. This study has applied the influence of the hybrid functional of three-parameter basis set of B3LYP (Becke, Lee, Yang, Parr) within the framework of DFT upon theoretical calculations [85, 86].

The popular B3LYP (Becke, three-parameter, Lee–Yang–Parr) exchange–correlation functional is [87–89]:

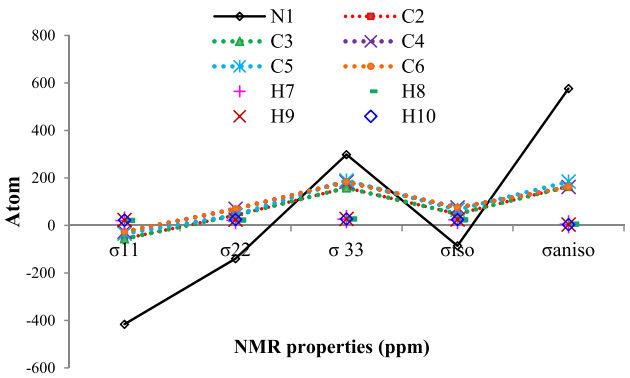

Fig. 1 The NMR plot of isotropic (σ_{iso}), anisotropic (σ_{aniso}) and eigenvalue shielding tensors (σ_{11}, σ_{22}, σ_{33}) calculated by level of theory B3LYP/6–31 + G*

$$E_{XC}^{B3LYP} = (1-\alpha)E_x^{LSDA} + \alpha E_x^{HF} + b\Delta E_x^{B} + (1-c)E_c^{LSDA} + cE_c^{LYP} \quad (6)$$

where $\alpha = 0.20, b = 0.72, c = 0.81$ is a generalized gradient approximation: the Becke exchange functional [85] and the correlation functional of Lee, Yang and Parr [86] for B3LYP and E_c^{LSDA} is the VWN local spin density approximation to the correlation functional [90].

The Al (111)-surface has been constructed by rigid system and Z-Matrix format of which a blank line has been placed and after that the following information has been illustrated. The rigid PES has been performed at B3LYP/6–31 + G* for Pyridine and its family (2-Methylpyridine, 3-Methylpyridine, 4-Methylpyridine and 2, 4-Dimethylpyridine) adsorbed onto the Al (111)-surface using Gaussian 09 program package [75]. For Al (111), the small energy difference between the formation of Al (111)- inhibitor complexes can direct us to a pretty coated surface for preventing the corrosion.

Results and Discussion

Inhibitors usually only reduce corrosion; but in some cases, like closed water systems, proper inhibition can virtually eliminate corrosion. Most inhibitors prevent or reduce corrosion of aluminum by either anodic or cathode reactions. Chromates suppress the anodic reactions and Chromate conversion coatings have been a widely used inhibitor for aluminum sheets.

In recent years, use of Chromates has decreased because of concerns for personnel and environmental toxicity. If anodic inhibitors are used in insufficient amounts, they may only restrict corrosion to fewer sites and actually increase corrosion

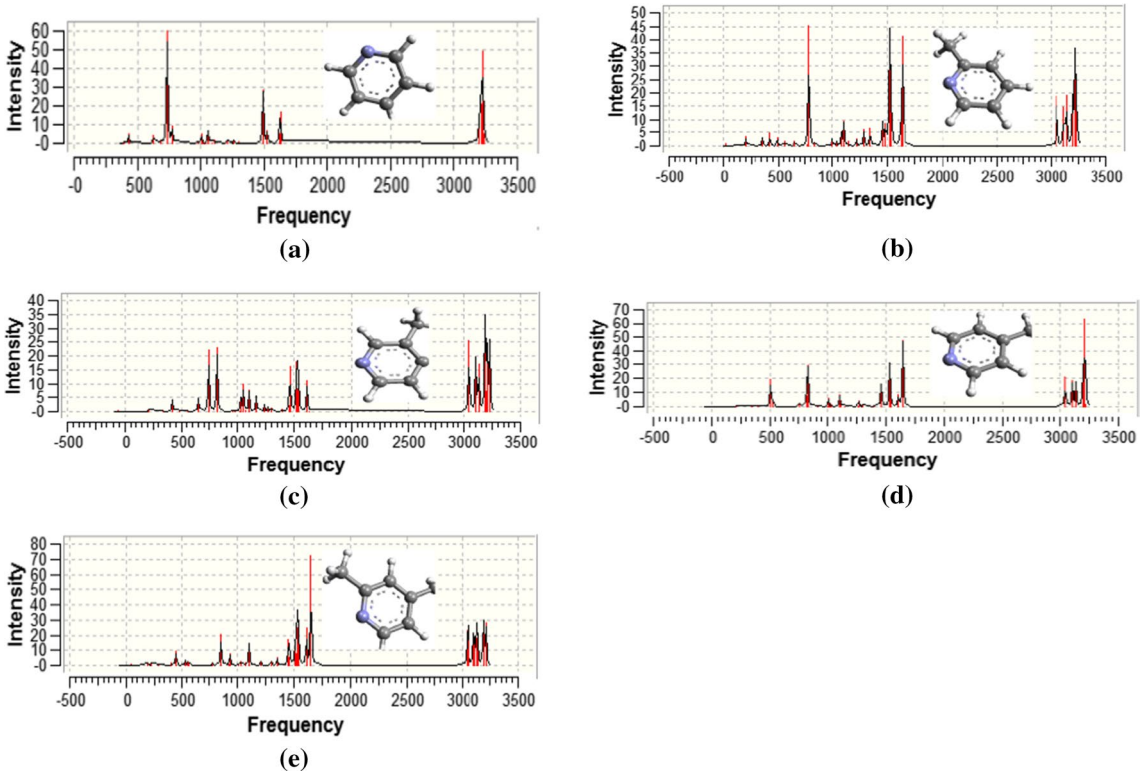

Scheme 2 Changes of IR intensity (km/mol) versus frequency (cm^{-1}) through the IR spectra for **a** Pyridine, **b** 2-Methylpyridine, **c** 3-Methylpyridine, **d** 4-Methylpyridine and **e** 2, 4-Dimethylpyridine using B3LYP/6–31 + G* calculations

Table 2 Calculated functions of harmonic frequencies (cm^{-1}), IR intensities (km/mol), Dipole Moments (μ, Debye) and ΔG, ΔH in kcal/mol and ΔS in cal/mol.K^{-1} at 300 K

Compounds	Normal mode	Intensity (km/mol)	Frequency (cm^{-1})	$\Delta G \times 10^{-3}$ (kcal/mol)	$\Delta H \times 10^{-3}$ (kcal/mol)	ΔS (cal/K.mol)	μ (Debye)
Pyridine	5	59.7903	734.6462	− 155.7165	− 155.6960	68.502	2.4840
	19	28.2186	1491.9495				
	22	16.3688	1629.2859				
	26	48.8404	3223.9243				
2-Methylpyridine	9	45.3516	781.7032	− 180.3696	− 180.3459	79.498	2.0399
	25	40.7927	1518.8941				
	29	41.2279	1639.3798				
	35	32.9596	3216.9408				
3-Methylpyridine	9	23.0361	817.1902	− 180.3665	− 180.3445	73.611	2.6698
	25	17.8787	1525.2042				
	30	25.4554	3043.2467				
	33	31.7158	3186.7542				
	36	24.4846	3227.0239				
4-Methylpyridine	10	29.3105	828	− 180.3669	− 180.3450	73.599	2.9839
	29	46.9895	1647.2223				
	30	21.0188	3044.0952				
	35	63.2199	3211.9458				
2, 4-Dimethylpyridine	13	20.3792	853.6878	− 205.0196	− 204.9947	83.596	2.5234
	33	24.8782	1533.2415				
	36	72.0421	1651.8226				
	37	23.3950	3043.1158				
	43	20.9553	3191.5476				
	45	28.1390	3215.1544				

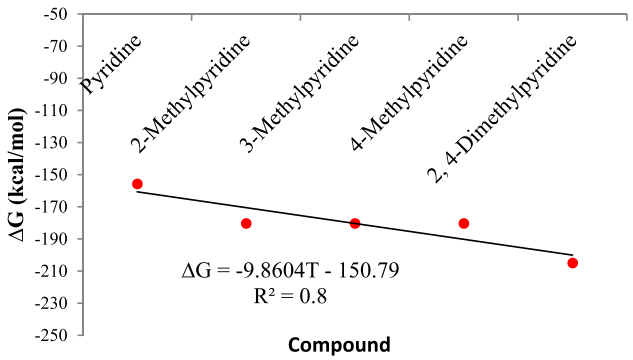

Fig. 2 The changes of Gibbs Free energy for Pyridine and four derivatives of 2-Methylpyridine, 3-Methylpyridine, 4-Methylpyridine and 2, 4-Dimethylpyridine at 300 K

at those localized sites. Most other inhibitors such as phosphates, silicates, nitrates, nitrites, benzoates, N-heterocyclic compounds and others have been used either alone or combination, affect the cathode reactions. Inhibitors of this type have been applied to effectively treat water systems, particularly closed systems. In this paper, the electronic structure of both inhibitor and aluminum-surface is important. The efficiency of an organic inhibitor of metallic corrosion does not only depend on the structure of the inhibitor molecule, but also characteristics of the environment in which it acts, on the nature of the metal and the other experimental conditions. Under certain conditions of the experiment, the electronic structure of the organic inhibitors has a key influence on the corrosion inhibition efficiency to the metal. In this model, the adsorption molecule has been adsorbed at the Al (111)-lattice in an inclined state.

We have estimated the distance between N atom in the pyridine ring and its derivatives and aluminum atom in the Al (111)-lattice. It has been shown that the pyridine ring and its derivatives have three double bonds including six electrons which are sufficient for aromatic ring formation without involving the lone pair electrons of the nitrogen atom. However, we cannot ignore that the nitrogen atom has a higher electronegativity than the carbon atoms.

Then the adsorption model of pyridine and its derivatives on the Al (111)-lattice has been optimized by Gaussian03 [75]. The stabilization Energy, E_s, is given as:

$$E_s = E_p - E_r \tag{7}$$

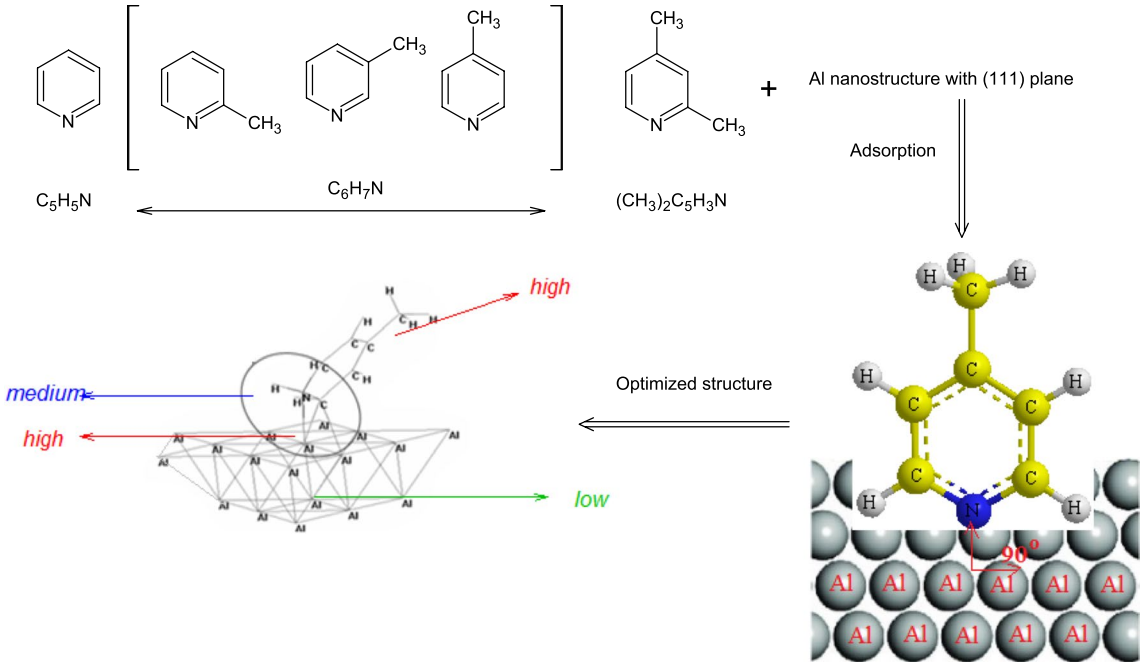

Scheme 3 The mechanism of the adsorption of pyridine and its family (2-Methylpyridine, 3-Methylpyridine, 4-Methylpyridine and 2,4-Dimethylpyridine) onto Al(111) metal surface based on optimized coordination of adsorption on the Al(111) metal surface

$$E_s^+ = E_p^+ - E_r^+ \quad (8)$$

where E_p represents the total energy of the given adsorption model consisting of non-protonated pyridine by its derivatives and the Al (111)-lattice, and E_r is the sum of the total energy of the free non-protonated molecule of the inhibitor and the energy of the Al (111)-lattice without interaction. Besides, E_s^+ shows the protonated stabilization energy; E_p represents the total energy of the given adsorption model consisting of protonated pyridine by its derivatives and the Al(111)-lattice, and E_r is the sum of the total energy of the free protonated molecule of the inhibitor and the energy of the Al(111)-lattice without interaction.

Other calculated electronic properties include the net atomic charge (Q), the change value of the net charge of the ─NH^+ group in the pyridine ring (ΔQ_{NH^+}), the net charge change of the Al- lattice ($\Delta Q_{Al(111)\text{-lattice}}$), the adsorption distance (R), adsorption angle (A), and the adsorption dihedral angle (D).

Metal (111) Surface Models

It has been investigated two model surfaces based on a unit cell of 3, (111) layers using a vacuum of 5, layers through the *z*-axis; the uppermost layer is allowed to relax in the computation, but the lower 2, layers are kept fixed. Using particle-size-dependent Al reactivity, it has been discovered that the adsorption energy of small molecules doesn't depend on the layers if there are more than 2, layers in the simulation. The surface constant applied to produce the model calculated at the PBE/PAW basis sets of theory consist of Electron density adsorption of imidazole / Al(111)/ slab complexes through different orientation [79–84].

Adsorbed Molecules on the Al (111) Surface

It has been investigated the suitability of each Al (111)-lattice model for describing interactions with adsorbents by considering the adsorption energy of the Pyridine and four derivatives of 2-Methylpyridine, 3-Methylpyridine, 4-Methylpyridine and 2, 4-Dimethylpyridine. This is also of importance for catalysis, as for surface reactions there is usually a close correlation between binding energies and activation energies. For these molecules, the lone pair of the deprotonated nitrogen atom that is not involved in the aromatic system is the most reactive site and thus the most likely site to bind to Al-surface. After optimizing Al(111) interface (adsorption and first Al layer), we obtain an N–Al distance of 2.30 Å for the smaller Al(111)- surface.

Charge Density Analysis

For observing the interaction between the pyridine, its family and the Al (111) surface, we have calculated the charge density difference (CDD) for the pyridine and its family

molecules at different adsorption sites for the large Al(111) surface model. The CDD is defined as:

$$\Delta Q_{ads} = Q_{adsorbate/surface} - Q_{surface} - Q_{adsorbate} \quad (9)$$

where $Q_{adsorbate/surface}$ is the charge density of the adsorption system; $Q_{surface}$ and $Q_{adsorbate}$ are the charge densities of the non-interacting surface and that of the adsorption, respectively. It has been modeled Pyridine, 2-Methylpyridine, 4-Methylpyridine and 2, 4-Dimethylpyridine as protonated compounds in hydrochloric acid (HCl) as weak bases (Table 3 and Fig. 3a, b). According to the values in Table 3, the charge changes of —NH^+ group ($\Delta Q_{NH}{}^+$) of the protonated Pyridine, 2-Methylpyridine, 4-Methylpyridine and 2, 4-Dimethylpyridine have been valued.

Non-Protonated Pyridine and its Derivatives

The stability energy (E_s), adsorbent energy (E_{ads}), metal surface energy ($E_{Al/surf}$), and adsorption energy ($E_{ads/surf}$) have been measured for non-protonated Pyridine, 2-Methylpyridine, 4-Methylpyridine and 2, 4-Dimethylpyridine (Table 4 and Fig. 4):

$$E_s = E_{ads/surf} - \left(E_{Al/surf} + E_{ads}\right) \quad (10)$$

Figure 4 has shown that stability energy of Pyridine, 3-Methylpyridine, 2-Methylpyridine, respectively has the optimized amount in these non-protonated compounds. The optimized geometry coordination of bond length (R), bond angle (A) and dihedral angle (D) for Pyridine, and four derivatives has been calculated (Table 5). Then linear regressions have been measured with the inhibition efficiencies (η) versus the change value of the net charge ($\Delta \mathbf{Q_N}$) of the –N group ($R^2 = 0.7072$) in the Pyridine ring and four derivatives of 2-Methylpyridine, 3-Methylpyridine, 4-Methylpyridine and 2, 4-Dimethylpyridine (Fig. 5).

Protonated Pyridine and its Derivatives

The stability energy ($E_s{}^+$), adsorbent energy (E_{ads}), metal surface energy ($E_{Al/surf}$), and adsorption energy ($E_{ads/surf}$) have been measured for protonated Pyridine, 2-Methylpyridine, 4-Methylpyridine and 2, 4-Dimethylpyridine (Table 6 and Fig. 6a, b).

$$E_s^+ = E_{ads/surf} - \left(E_{Al/surf} + E_{ads}\right) \quad (11)$$

It has been modeled the Pyridine and four derivatives of 2-Methylpyridine, 3-Methylpyridine, 4-Methylpyridine and 2, 4-Dimethylpyridine as protonated compounds in hydrochloric acid (HCl) as weak bases. The optimized geometry coordination of bond length (R), bond angle (A) and dihedral angle (D) for Pyridine, and four derivatives has been calculated (Table 7 and Fig. 6a).The charge fluctuation of —NH^+ group ($\Delta \mathbf{Q_{NH}}^+$) via $E_S{}^+$ for protonated Pyridine and four derivatives of 2-Methylpyridine, 3-Methylpyridine, 4-Methylpyridine and 2,4-Dimethylpyridine have been shown (Fig. 6b). The linear regression in Fig. 6b ($R^2 = 0.6245$) has indicated a medium correlation among adsorption of these compounds onto Al (111) surface.

Since the —NH^+ group as an electron acceptor of the protonated pyridine ring has a positive charge, it accepts the electron of the aluminum atoms easily. The charge of the Al (111)-lattice is affected and turns positive by the adsorption, so the electronic transfer must be from the Al atom to the organic inhibitor through the frontier orbital of the interface when the inhibitor is adsorbed onto the Al (111)-lattice (Fig. 6b).

Table 3 The calculated electronic charges of non-protonated Pyridine, 2-Methylpyridine, 4-Methylpyridine and 2, 4-Dimethylpyridine

Inhibitor	$Q_{Al\text{-}surf} \times 10^{-2}$	$Q'_{Al\text{-}surf} \times 10^{-2}$	$\Delta Q_{Al\text{-}surf} \times 10^{-2}$	$Q_N \times 10^{-2}$	$Q'_N \times 10^{-2}$	$\Delta Q_N \times 10^{-2}$
Pyridine	2.85	59.79	56.93	−38.96	−75.21	−36.25
2-Methylpyridine		56.65	53.79	−41.40	−79.40	−37.99
4-Methylpyridine		64.70	61.84	−39.03	−76.16	−37.13
2, 4-Dimethylpyridine		58.95	56.10	−41.58	−79.40	−37.83
b Optimized electronic charges of protonated Pyridine, 2-Methylpyridine, 4 Methylpyridine and 2, 4-Dimethylpyridine						
Inhibitor	$Q_{Al\text{-}surf} \times 10^{-2}$	$Q'_{Al\text{-}surf} \times 10^{-2}$	$\Delta Q_{Al\text{-}surf} \times 10^{-2}$	$Q_{NH}{}^+ \times 10^{-2}$	$Q'_{NH}{}^+ \times 10^{-2}$	$\Delta Q_{NH}{}^+ \times 10^{-2}$
Pyridine	2.85	1.14	1.11	−12.95	−44.90	−31.95
2-Methylpyridine		1.08	1.05	−16.27	−47.60	−31.32
4-Methylpyridine		1.12	1.09	−13.90	−44.41	−30.51
2, 4-Dimethylpyridine		1.07	1.04	−17.04	−47.53	−30.49

Q = charge value before adsorption

Q′ = charge value after adsorption

ΔQ = Q′—Q

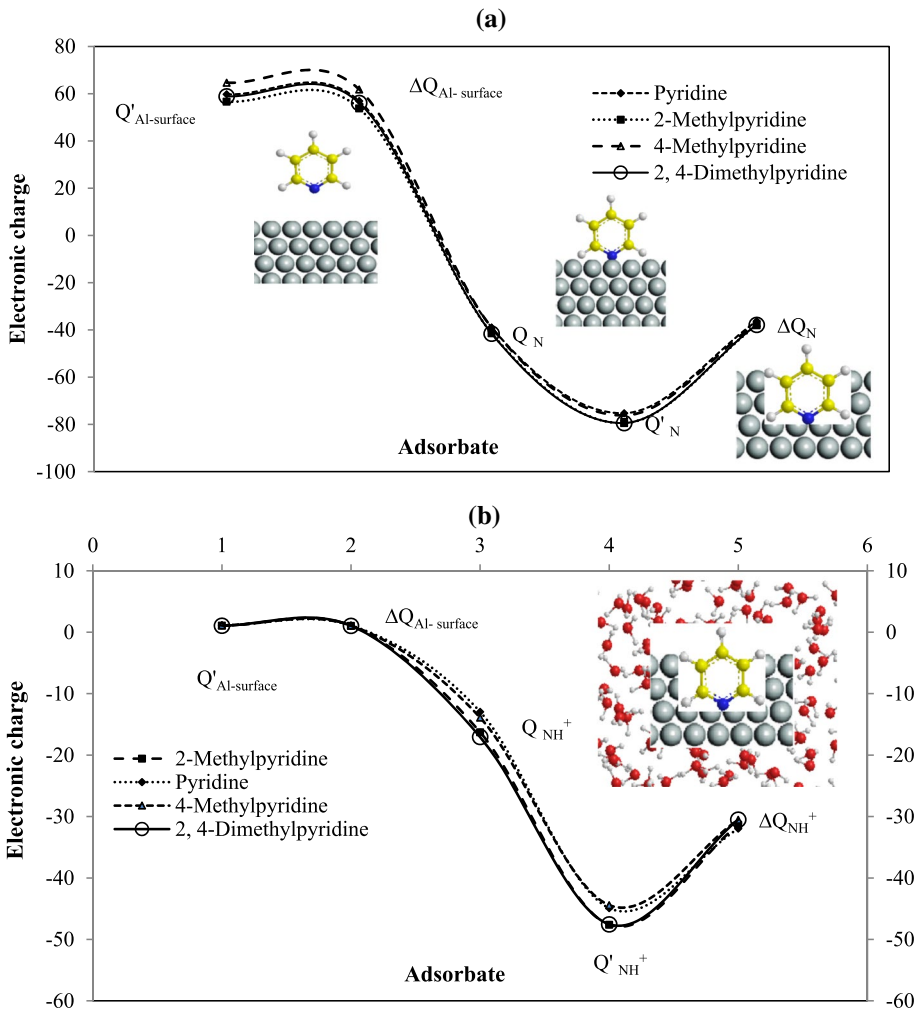

Fig. 3 Calculated electronic charge of **a** the non-protonated **b** protonated of Pyridine, 2-Methylpyridine, 4-Methylpyridine and 2, 4-Dimethylpyridine

The N-Al adsorption distance has obtained from the optimization calculations (Table 7). These results have exhibited that the N-Al covalent bond in Fig. 6a between the inhibitor and the Al (111)-lattice has been formed. ΔQ_{NH}^{+} represents the amount of the net charge of the ─NH^+ group in the pyridine ring and its family group. $\Delta Q_{NH}^{+} = Q'_{NH}^{+} — Q_{NH}^{+}$; Q'_{NH}^{+} is the charge of the ─NH^+ group when the inhibitor is adsorbed onto the Al (111)-lattice and Q_{NH}^{+} ($=Q_N + Q_H^+$) is the net charge of the ─NH^+ group of the protonated pyridine and its derivatives (Fig. 6b).

Table 4 Stability energy (kcal/mol) of non-protonated pyridine and its derivatives

Adsorption	$E_{Al/surf}$	E_{ads}	$E_{ads/surf}$	E_s	*η
Pyridine	−35.86	−248.12	−284.02	−19.9390	20.8
2-Methylpyridine		−287.41	−323.31	−25.3315	65.65
4-Methylpyridine		−287.42	−323.32	−19.4804	67.43
2, 4-Dimethyl-pyridine		−326.72	−362.62	−22.8180	99

*η is the inhibition efficiency of pyridine and its derivatives [91]

Co-Adsorption Modeling with Hydrogen Atom, Cl^- and NO_3^- Anions in Acidic Media

The optimized result by the DFT/B3LYP/6–31 + G* level of theory has indicated that Pyridine, 2-Methylpyridine, 3-Methylpyridine, 4-Methylpyridine and 2,4-Dimethylpyridine can be adsorbed onto the Al(111)-lattice in the inclined states and the inclined angles of the inhibitors adsorbed on the Al(111)-lattice are different from each other. Their common point is the N atom in the pyridine ring close to the Al (111)-lattice.

To investigate the relationship between the adsorption and its influence on the hydrogen entry onto the Al (111)-surface, the co-adsorption of protonated pyridine with adsorbed hydrogen and Cl^- has been modeled. The Al (111)-lattice with H^+ and Cl^- has been employed as the substrate for modeling the co-adsorption. The results of the optimized calculation have been shown in Table 8.

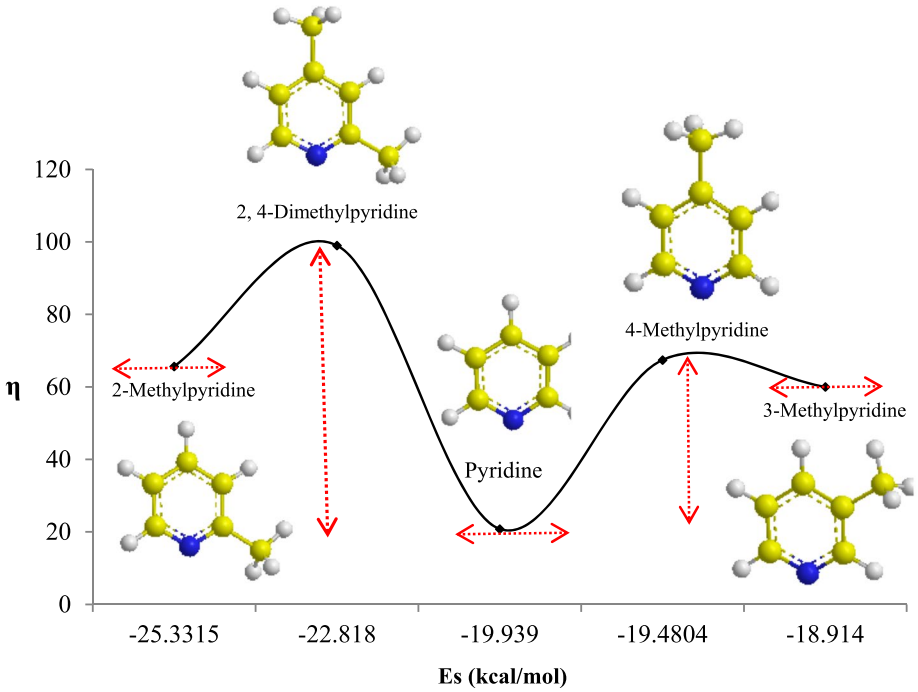

Fig. 4 The changes of inhibition efficiencies (η) versus calculated stabilization energies (E_s) for non-protonated Pyridine and four derivatives of 2-Methylpyridine, 3-Methylpyridine, 4-Methylpyridine and 2, 4-Dimethylpyridine

Table 5 The calculated parameters of non-protonated pyridine and its derivatives

Inhibitor	$R_{N\text{-}Al(1)}$ (Å)	$A_{C(20)\text{-}N(19)\text{-}Al(1)}$ (o)	$D_{C(20)\text{-}N(19)\text{-}Al(1)\text{-}Al(4)}$ (o)
Pyridine	1.7774	88.8968	−11.8967
2-Methylpyridine	1.7945	146.5161	−32.2029
3-Methylpyridine	1.7790	142.8958	84.9337
4-Methylpyridine	1.7707	144.2381	15.1716
2, 4-Dimethylpyridine	1.7896	149.0195	91.5205

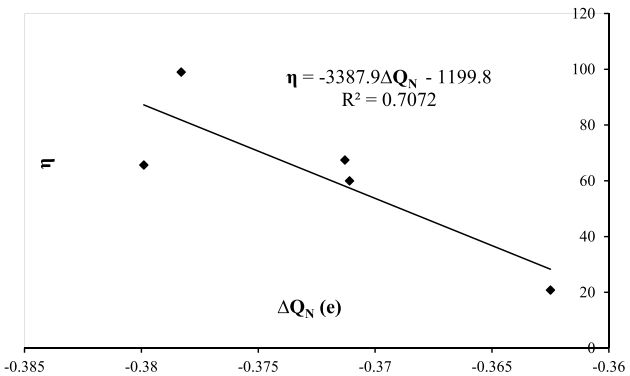

Fig. 5 The linear regression of inhibition efficiencies (η) versus the net charge of the ─N group (ΔQ_N) in the non-protonated Pyridine ring and four derivatives of 2-Methylpyridine, 3-Methylpyridine, 4-Methylpyridine and 2, 4-Dimethylpyridine

It might be the adsorption of Cl^- onto the Al (111)-surface causes increasing the negative charge on the Al (111)-lattice, which improves the interaction between protonated pyridine and the Al (111)-lattice. We can conclude that the adsorption of the inhibitor is possible only at a lattice partially covered with solution of H^+ and Cl^-. Finally, the stability energy (E_s^+) of protonated Pyridine, 2-Methylpyridine, 3-Methylpyridine, 4-Methylpyridine and 2, 4-Dimethylpyridine onto Al(111)-lattice have been investigated through co-adsorption model in the solution of H^+, Cl^- and NO_3^- (Tables 9 and 10 and Fig. 7).

Table 6 Stability energy (kcal/mol) of protonated pyridine and its derivatives

Adsorbate	$E_{Al/surf}$	E_{ads}	$E_{ads/surf}$	E_s^+
Pyridine	−35.86	−248.47	−284.42	−53.60
2- Methylpyridine		−287.78	−323.72	−43.31
4- Methylpyridine		−287.79	−323.73	−42.85
2,4-Dimethylpyridine		−327.11	−363.02	−31.57

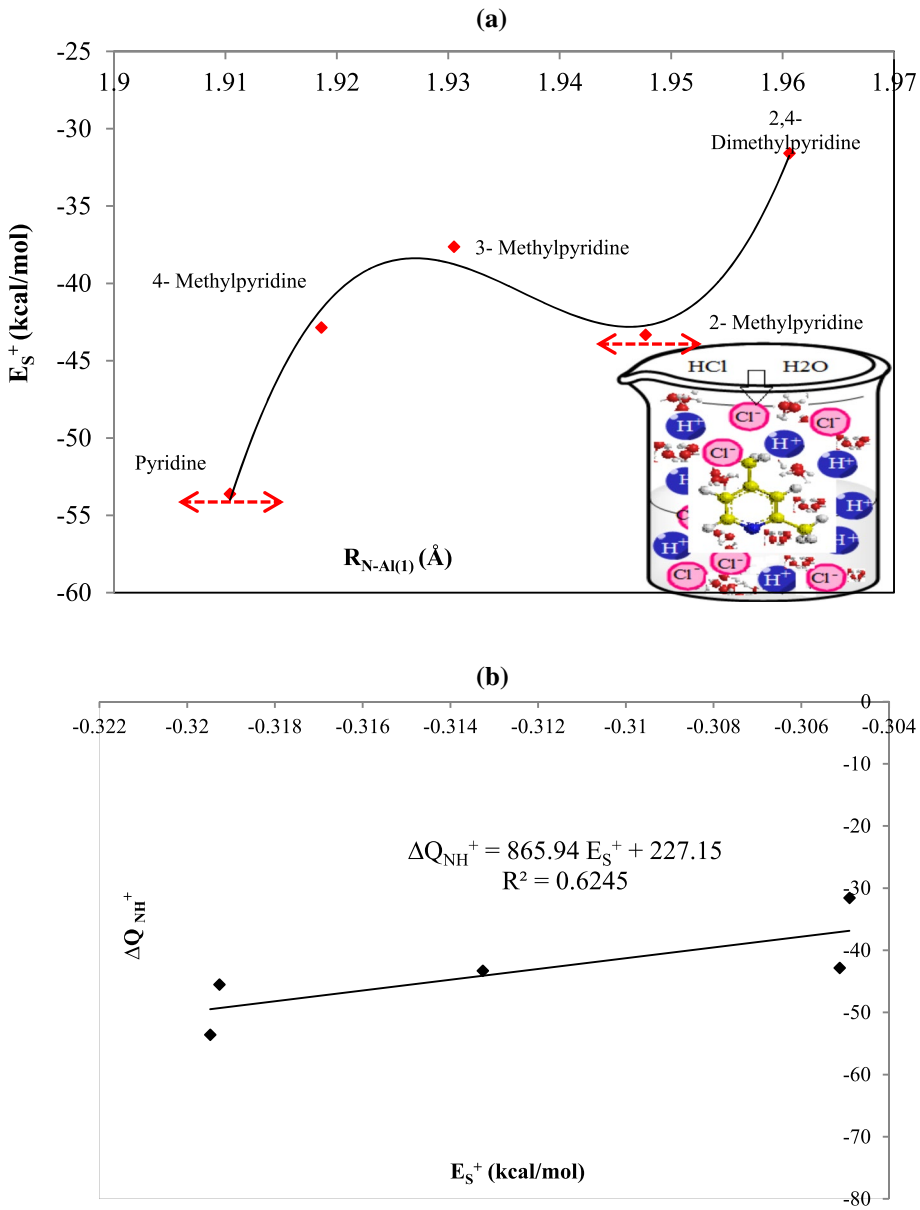

Fig. 6 **a** Calculated stabilization energies (E_S^+) versus bond length between nitrogen atoms and Al (1), $R_{N\text{-}Al(1)}$ (Å), on co-adsorption model with hydrogen atom and Cl^- anion for Pyridine and four derivatives of 2-Methylpyridine, 3-Methylpyridine, 4-Methylpyridine and 2, 4-Dimethylpyridine. **b** The charge changes of $-NH^+$ group (ΔQ_{NH}^+) of the protonated Pyridine and four derivatives of 2-Methylpyridine, 3-Methylpyridine, 4-Methylpyridine and 2, 4-Dimethylpyridine versus protonated stability energy ($E_S.^+$ kcal/mol)

Table 7 The calculated parameters of Pyridine, 2-Methylpyridine, 3-Methylpyridine, 4-Methylpyridine and 2,4-Dimethylpyridine in hydrochloric acid (HCl)

Adsorption	$R_{N\text{-}Al(1)}$(Å)	$A_{C(20)\text{-}N(19)\text{-}Al(1)}$ (o)	$D_{C(20)\text{-}N(19)\text{-}Al(1)\text{-}Al(4)}$ (o)
Pyridine	1.9104	86.7495	−10.9617
2-Methylpyridine	1.9477	132.5616	−54.3351
3-Methylpyridine	1.9212	127.136	59.6346
4-Methylpyridine	1.9186	126.513	−7.8007
2,4-Dimethylpyridine	1.9606	134.3384	63.1696

Conclusion

The adsorption and diffusion of Pyridine, 2-Methylpyridine, 3-Methylpyridine, 4-Methylpyridine and 2, 4-Dimethylpyridine onto Al(111)-lattice have been investigated using ONIOM method with high, medium and low levels of 6–31 + G*/LANL2DZ, semi-empirical and MM2 basis sets, respectively by program package Gaussian 09.

In this work, the efficiency of the organic inhibitors as the metallic coating has been studied through the electronic,

Table 8 The optimized geometry coordination of co-adsorption model for Pyridine, 2-Methylpyridine, 3-Methylpyridine, 4-Methylpyridine and 2,4-Dimethylpyridine with H^+ cation and Cl^- anion

Adsorbate	$R_{N\text{-}Al(1)}$(Å)	$A_{C(20)\text{-}N(19)\text{-}Al\ (1)}$	$D_{C(20)\text{-}N(19)\text{-}Al(1)\text{-}Al(4)}$	$R_{H\text{-}Al(8)}$ (Å)	$R_{Cl\text{-}Al(9)}$ (Å)
Pyridine	1.9039	88.226	−8.2088	1.4234	2.0914
2-Methylpyridine	1.9411	134.2746	−43.3963	1.4148	2.094
3-Methylpyridine	1.9067	128.1313	47.5393	1.4232	2.0847
4-Methylpyridine	1.9107	127.7998	1.4097	1.4219	2.0916
2,4-Dimethylpyridine	1.9557	137.2764	43.7559	1.4233	2.0827

Table 9 Stability energy (kcal/mol) of the co-adsorption model with adsorbed hydrogen and Cl^- for Pyridine, 2-Methylpyridine, 3-Methylpyridine, 4-Methylpyridine and 2, 4-Dimethylpyridine onto Al(111)-lattice

Adsorbate	$E_{Al/surf}$	Eads	$E_{Cl\text{-}/surf}$	$E_{ads/surf}$	E_s^+
Pyridine	−35.86	−248.47	−460.25	−745.20	−385.25
2-Methylpyridine		−287.78		−784.50	−374.51
4- Methylpyridine		−287.79		−784.49	−371.78
2,4- Dimethylpyridine		−327.10		−823.78	−355.60

$E_s = E_{Al/surf/H+/Cl^-/ads} - (E_{Al/surf} + E_{H^+} + E_{Cl^-} + E_{ads})$

Table 10 Stability energy (kcal/mol) of the co-adsorption model with adsorbed hydrogen and NO_3^- for Pyridine, 2-Methylpyridine, 3-Methylpyridine, 4-Methylpyridine and 2, 4-Dimethylpyridine onto Al (111)-lattice

Adsorbate	$E_{Al/surf}$	E_{ads}	$E_{NO3^-/surf}$	$E_{ads/surf}$	E_s^+
Pyridine	−35.86	−248.47	−280.22	−565.16	−377.42
2- Methylpyridine		−287.79		−604.46	−367.53
4- Methylpyridine		−287.80		−604.58	−367.87
2,4- Dimethylpyridine		−327.09		−643.74	−347.77

$E_s = E_{Al/surf/H+/NO3^-/ads} - (E_{Al/surf} + E_{H^+} + E_{NO3^-} + E_{ads})$

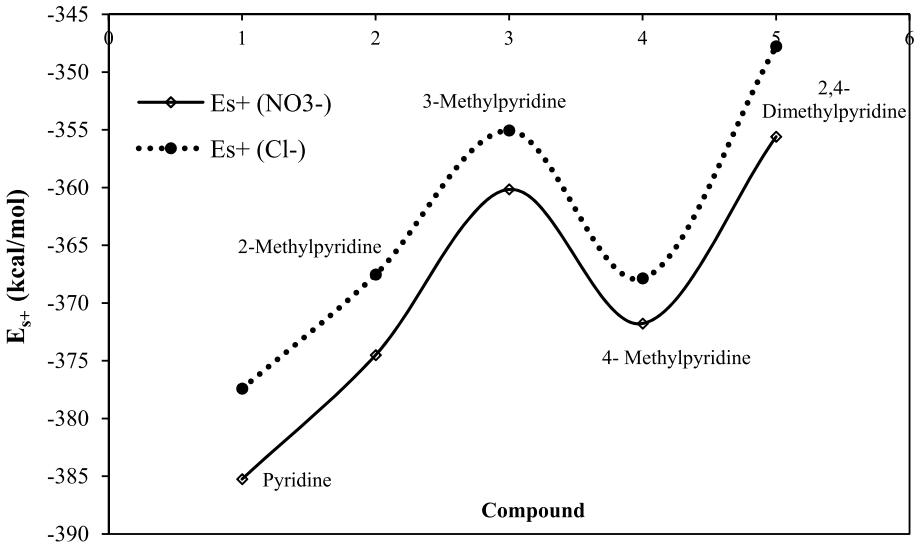

Fig. 7 Calculated stabilization energies (E_S^+) of Pyridine and four derivatives of 2-Methylpyridine, 3-Methylpyridine, 4-Methylpyridine and 2, 4-Dimethylpyridine in through co-adsorption model in the solution of H^+, Cl^- and NO_3^-

thermodynamic features and characteristics of the environmental condition on Pyridine, 2-Methylpyridine, 3-Methylpyridine, 4-Methylpyridine and 2, 4-Dimethylpyridine adsorbed by aluminum-surface.

An elaborate search for local minima in the adsorption potential energy landscape reveals that the intact pyridine adsorbs with the aromatic ring parallel to the surface. In the preferred path, the pyridine and its derivatives remains

parallel to the surface while performing small single rotational steps with a carbon–carbon double bond hinged above a single Al atom.

The inhibition properties of the protonated pyridine and derivatives molecules are related to the sum of the net charge and the π charge of the six-ring, respectively. Pyridine and its derivatives have been adsorbed on the lattice of the Al electrode mainly in their protonated forms. The most probable adsorption model of the inhibitors is one in which the N atom of the pyridine ring is close to the aluminum atom of the Al (111)-lattice in an inclined state. Moreover, it has been concluded that the adsorption of Pyridine and its derivatives including 2-Methylpyridine, 3-Methylpyridine, 4-Methylpyridine and 2, 4-Dimethylpyridine adsorbed by aluminum-surface.

As the organic heterocyclic compounds might be possible only at a surface partly covered with solution of H^+ and Cl^-. The stability energy ($E_s{}^+$) in the protonated pyridine, 2-Methylpyridine, 3-Methylpyridine, 4-Methylpyridine and 2, 4-Dimethylpyridine onto Al (111)-lattice has indicated the validity of co-adsorption model in the solution of H^+, Cl^- and $NO_3{}^-$ ions.

References

1. G. Tarantella (1991). *Corrosion* **47**, 410.
2. G. Schmitt (1984). *Corros. J.* **19**, 165.
3. J. O. M. Bockris and B. Yang (1991). *J. Electrochem. Soc.* **138**, 2237.
4. F. B. Growcock and V. R. Lopp (1988). *Corros. Sci.* **28**, 397.
5. M. Bartos and N. Hackerman (1992). *J. Electrochem. Soc.* **139** (3), 429.
6. F. Zucchi, G. Trabanelli, and G. Brunoro (1992). *Corros. Sci.* **33** (1), 135.
7. S. L. Graaese (1988). *Corrosion.* **44**, 222.
8. A. B. Tadros and B. A. Abdenaby (1988). *J. Electroanal. Chem.* **246**, 433.
9. B. Mernari, H. Elattari, M. Traisnel, F. Bentiss, and M. Lagreence (1998). *Corros. Sci.* **40**, 391.
10. F. Bentiss, M. Lagreence, and M. Traisnel (1999). *Corros. Sci.* **41**, 789.
11. F. Bentiss, M. Traisnel, and M. Lagreence (2000). *Corros. Sci.* **42**, 127.
12. D. Xue Ging (1990). *J. Appl. Surf. Sci.* **40**, 327.
13. D. Chadwick and T. Hashemi (1978). *Corros. Sci.* **20**, 88.
14. J. J. Xue Gadding (1991). *J. Phys. Chem.* **95**, 7380.
15. Khaleghian, M.; Zahmatkesh, M.; Mollaamin, F.; Monajjemi, M. (2011) Investigation of Solvent Effects on Armchair Single-Walled Carbon Nanotubes: A QM/MD Study. Fullerenes Nanotubes and Carbon Nanostructures 19
16. L. Ming-Dao, B. Gang, K. Fu-Gui, Y. Lu-An, and Y. Xiao-Ci (1996). *Acta Chemica.* **12** (9), 859.
17. L. Ming-Dao, Y. Lu-An, W. Qing-Yu, Y. Xiao-Ci, Y. Xiao-Dong, and Z. Jin-Yun (1996). *J. Chinese Soc. Corrosion Protec.* **16** (3), 195.
18. C. Wei (2019). Electrochemical deposition of aluminum. *Technol. Innov. Appl.* **18**, 80–81.
19. H. M. Yang, Z. X. Qiu, and G. Zhang, *Low Temperature Aluminum Electrolysis* (Northeast University Press, Shenyang, China, 2009).
20. H. M. Lu and Z. X. Qiu (1997). Research progress of low temperature aluminum electrolysis. *Light Metals* **4**, 24.
21. M. Monajjemi, M. T. Baie, and F. Mollaamin (2010). Interaction between threonine and cadmium cation in [Cd(Thr) n]2+ (n = 1–3) complexes: density functional calculations. *Russian Chemical Bulletin* **59**, 886–889.
22. F. Mollaamin and M. Monajjemi (2015). Harmonic linear combination and normal mode analysis of semiconductor nanotubes vibrations. *J. Comput. Theor. Nanosci.* **12**, 1030–1039.
23. P. Wasserscheid and T. Welton, *Ionic Liquids in Synthesis; John Wiley & Sons: Hoboken* (NJ, USA, 2008).
24. M. Zhang, V. Kamavarum, and R. G. Reddy (2003). New electrolytes for aluminum production. *Ionic Liquids. JOM* **55**, 54.
25. G. C. Tian, J. Li, and Y. X. Hua (2009). Application of ionic liquids in metallurgy of nonferrous metals. *Chin. J. Process Eng.* **9**, 200.
26. G. C. Tian, J. Li, and Y. X. Hua (2010). Application of ionic liquids in hydrometallurgy of nonferrous metals. *Trans. Nonferrous Met. Soc. China* **20**, 513.
27. M. Monajjemi, S. Afsharnezhad, M. R. Jaafari, S. Mirdamadi, F. Mollaamin, and H. Monajemi (2008). Investigation of energy and NMR isotropic shift on the internal rotation Barrier of Θ4 dihedral angle of the DLPC: A GIAO study. *Chemistry* **17**, 55–69.
28. G. C. Tian (2019). Ionic liquids as green electrolytes for Aluminum and Aluminum-alloy production. *Mater. Res. Found.* **54**, 249.
29. X. W. Zhong, T. Xiong, J. Lu, and Z. N. Shi (2014). Advances of electro-deposition and aluminum refining of aluminum and aluminum alloy in ionic liquid electrolytes system. *Nonferrous Met. Sci. Eng.* **5**, 44.
30. Y. Zheng, Q. Wang, Y. J. Zheng, and H. C. Lv (2015). Advances in research and application of aluminum electrolysis in ionic liquid systems. *Chin. J. Process Eng.* **15**, 713.
31. V. Fleury, J. H. Kaufman, and D. B. Hibbert (1994). Mechanism of a morphology transition in ramified electrochemical growth. *Nature* **367**, 435.
32. G. Yue, X. Lu, Y. Zhu, X. Zhang, and S. Zhang (2009). Surface morphology, crystal structure and orientation of aluminum coatings electrodeposited on mild steel in ionic liquid. *Chem. Eng. J.* **147**, 79.
33. A. P. Abbott, F. Qiu, H. M. Abood, M. R. Ali, and K. S. Ryder (1862). Double layer, diluent and anode effects upon the electrodeposition of aluminum from chloroaluminate based ionic liquids. *Phys. Chem. Chem. Phys.* **2010**, 12.
34. M. Monajjemi, L. Mahdavian, F. Mollaamin, and M. Khaleghian (2009). Interaction of Na, Mg, Al, Si with carbon nanotube (CNT): NMR and IR study. *Russian J. Inorg. Chem.* **54**, 1465–1473.
35. M. Ueda, S. Hariyama, and T. Ohtsuka (2012). Al electroplating on the AZ121 Mg alloy in an EMIC-$AlCl_3$ ionic liquid containing ethylene glycol. *J. Solid State Electrochem.* **16**, 3423.
36. Q. Zhang, Q. Wang, S. Zhang, and X. Lu (2014). Effect of nicotinamide on electrodeposition of Al from aluminum chloride ($AlCl_3$)-1-butyl-3-methylimidazolium chloride ([BMIM]Cl) ionic liquids. *J. Solid State Electrochem.* **18**, 257.
37. M. Monajjemi, M. Khaleghian, N. Tadayonpour, and F. Mollaamin (2010). The effect of different solvents and temperatures on stability of single-Walled carbon nanotube: A Qm/Md study. *Int. J. Nanosci.* **09**, 517–529.
38. B. Ghalandari, M. Monajjemi, and F. Mollaamin (2011). Theoretical investigation of carbon nanotube binding to DNA in view of drug delivery. *J. Comput. Theor. Nanosci.* **8**, 1212–1219.
39. F. Mollaamin, M. Monajjemi, S. Salemi, and M. T. Baei (2011). A dielectric effect on normal mode analysis and symmetry of

BNNT Nanotube. *Fullerenes Nanotubes and Carbon Nanostruc.* **19**, 182–196.
40. N. Hackerman and A. C. Makrides (1954). *Ind. Engng. Chem.* **46**, 523.
41. K. Aramaki, N. Hackerman, and J. Eleclrochem (1968). *Soc* **115**, 1007.
42. A.I. Altsybeeva, S.Z. Levin and A.P. Dorokhov (1970) European Symposium on Corrosion Inhibitors, Ferrera 501
43. J. V. Barth, H. Brune, G. Ertl, and R. J. Behm (1990). Scanning tunneling microscopy observations on the reconstructed Au(111) surface: Atomic structure, long-range superstructure, rotational domains, and surface defects. *Phys. Rev. B.* **42**, 9307–9318.
44. D. Esken, S. Turner, O. I. Lebedev, G. van Tendeloo, and R. A. Fischer (2010). Au@ ZIFs: stabilization and encapsulation of cavity-size matching gold clusters inside functionalized zeolite imidazolate frameworks. *ZIFs. Chem. Mater.* **22**, 6393–6401.
45. F. Mollaamin, A. Ilkhani, N. Sakhaei, B. Bonsakhteh, A. Faridchehr, S. Tohidi, and M. Monajjemi (2015). Thermodynamic and solvent effect on dynamic structures of nano bilayer-cell membrane: hydrogen bonding study. *J. Comput. Theoretical Nanosci.* **12**, 3148–3154.
46. B. Liu and B. Smit (2010). Molecular simulation studies of separation of CO2/N2, CO2/CH4, and CH4/N2 by ZIFs. *J. Phys. Chem. C* **114**, 8515–8522.
47. S. Keskin (2010). Atomistic simulations for adsorption, diffusion, and separation of gas mixtures in zeolite imidazolate frameworks. *J. Phys. Chem. C* **115**, 800–807.
48. U. P. N. Tran, K. K. A. Le, and N. T. S. Phan (2011). Expanding applications of metal- organic frameworks: zeolite imidazolate framework ZIF-8 as an efficient heterogeneous catalyst for the knoevenagel reaction. *ACS Catal.* **1**, 120–127.
49. J. VandeVondele, M. Krack, F. Mohamed, M. Parrinello, T. Chassaing, and J. Hutter (2005). Quickstep: Fast and accurate density functional calculations using a mixed Gaussian and plane waves approach. *Comp. Phys. Comm.* **2**, 103–128.
50. A. Phan, C. J. Doonan, F. J. Uribe-Romo, C. B. Knobler, and O'keeffe, M., Yaghi, O. M. (2010). Synthesis, structure, and carbon dioxide capture properties of zeolitic imidazolate frameworks. *Acc. Chem. Res.* **43**, 58–67.
51. P. Hohenberg and W. Kohn (1964). Inhomogeneous electron gas. *Phys. Rev. B* **136**, B864–B871.
52. W. Kohn and L. J. Sham (1965). Self-consistent equations including exchange and correlation effects. *Phys. Rev.* **140**, A1133–A1138.
53. G. Lippert, J. Hutter, and M. Parrinello (1997). A hybrid Gaussian and plane wave density functional scheme. *Mol. Phys.* **92**, 477–487.
54. C. Hartwigsen, S. Goedecker, and J. Hutter (1998). Relativistic separable dual-space Gaussian pseudopotentials from H to Rn. *Phys. Rev. B* **58**, 3641–3662.
55. J. P. Perdew, K. Burke, and M. Ernzerhof (1996). Generalized Gradient Approximation Made Simple. *Phys. Rev. Lett.* **77**, 3865–3868.
56. J. VandeVondele and J. Hutter (2007). Gaussian basis sets for accurate calculations on molecular systems in gas and condensed phases. *J. Chem. Phys.* **127**, 114105–114109.
57. M. Monajjemi, M. Noei, and F. Mollaamin (2010). Design of fMet-tRNA and calculation of its bonding properties by quantum mechanics. *Nucleosides, Nucleotides & Nucleic Acids* **29**, 676–683.
58. M. Mavrikakis, P. Stoltze, and J. K. Nørskov (2000). Making gold less noble. *Catal. Lett.* **64** (101–106), 59.
59. A. Dal Corso (2013). Ab initio phonon dispersions of transition and noble metals: effects of the exchange and correlation functional. *J. Phys.; Condens Matter* **25**, 145401–145410.
60. L. J. Whitman, J. A. Stroscio, R. A. Dragoset, and R. J. Celotta (1991). Geometric and electronic properties of Cs structures on III-V (110) surfaces: From 1D and 2D insulators to 3D metals. *Phys. Rev. Lett.* **66**, 1338–1341.
61. M. A. A. Zadeh, H. Lari, L. Kharghanian, E. Balali, R. Khadivi, H. Yahyaei, F. Mollaamin, and M. Monajjemi (2015). Density functional theory study and anti-cancer properties of shyshaq plant. in view point of nano biotechnology. *J. Comput. Theoret. Nanosci.* **12**, 4358–4367.
62. H. Yildirim, T. Greber, and A. Kara (2013). Trends in adsorption characteristics of benzene on transition metal surfaces: role of surface chemistry and van der waals interactions. *J. Phys. Chem. C* **117**, 20572–20583.
63. A. Tahan, F. Mollaamin, and M. Monajjemi (2009). Thermochemistry and NBO analysis of peptide bond: Investigation of basis sets and binding energy. *Russian J. Phys. Chem. A* **83**, 587–597.
64. M. Hoefling, F. Iori, S. Corni, and K. E. Gottschalk (2010). The conformations of amino acids on a Gold(111) surface. *Chem. Phys. Chem.* **11**, 1763–1767.
65. K. Bakhshi, F. Mollaamin, and M. Monajjemi (2011). Exchange and correlation effect of hydrogen chemisorption on nano V(100) Surface: A DFT study by generalized gradient approximation (GGA). *J. Comput. Theoret. Nanosci.* **8**, 763–768. https://doi.org/10.1166/jctn.2011.1750.
66. B. Cordero, V. Gómez, A. E. Platero-Prats, M. Revés, J. Echeverría, E. Cremades, F. Barragán, and S. Alvarez (2008). Covalent radii revisited. *Dalton Trans.* **21**, 2832–2838.
67. A. van der Bondii (1964). Waals Volumes and Radii. *Phys. Chem.* **68**, 441–451.
68. H. Valencia, M. Kohyama, S. Tanaka, and H. Matsumoto (2008). Ab initio study of EMIM-BF_4 molecule adsorption on Li surfaces as a model for ionic liquid/Li interfaces in Li-ion batteries. *Phys. Rev. B* **78**, 205402.
69. H. Valencia, M. Kohyama, S. Tanaka, and H. Matsumoto (2009). Ab initio study of EMIM-BF_4 crystal interaction with a Li (100) surface as a model for ionic liquid/Li interfaces in Li-ion batteries. *J. Chem. Phys.* **131**, 244705.
70. J. Clarke-Hannaford, M. Breedon, A. S. Best, and M. J. Spencer (2019). The interaction of ethylammoniumtetrafluoroborate [$EtNH_3^+$][BF_4^-] ionic liquid on the Li (001) surface, towards understanding early SEI formation on Li metal. *Phys. Chem. Chem. Phys.* **21**, 10028–10037.
71. Q. Q. Zhang, *Study on Electrodeposition of Aluminum and Aluminum Alloy in Ionic Liquid* (University of Chinese Academy of Sciences, Beijing, China, 2014).
72. E. L. Kolsbjerg, M. N. Groves, and B. Hammer (2016). Pyridine adsorption and diffusion on Pt(111) investigated with density functional theory. *J. Chem. Phys.* **144**, 164112.
73. S. Shimizu, N. Watanabe, T. Kataoka, T. Shoji, N. Abe, S. Morishita, and H. Ichimura (2000). Pyridine and pyridine derivatives. *Ullmann's Encyclopedia of Industrial Chemistry Weinheim: Wiley-VCH*. https://doi.org/10.1002/14356007.a22_399.
74. E. J. O'Loughlin, S. J. Traina, and G. K. Sims (2000). Effects of sorption on the biodegradation of 2-methylpyridine in aqueous suspensions of reference clay minerals. *Environ. Toxicol. Chem.* **19** (9), 2168–2174. https://doi.org/10.1002/etc.5620190904.
75. Frisch, M.J.; Trucks, G.W.; Schlegel, H.B.; Scuseria, G.E.; Robb, M.A.; Cheeseman, J.R.; Scalmani, G.; et al. Gaussian 09, Revision B.01. **2010**. Gaussian Inc., Wallingford
76. A. Fry, K. Kwon, S. D. Komarneni, J. T. Kubicki, and K. Mueller (2006). Solid-state NMR and computational chemistry study of mononucleotides adsorbed to alumina. *Langmuir* **22**, 9281–9286.
77. M. Svensson, S. Humbel, R. D. J. Froese, T. Matsubara, S. Sieber, and K. Morokuma (1996). ONIOM: A Multilayered Integrated MO + MM method for geometry optimizations and single point energy predictions. A Test for diels−alder reactions and

Pt(P(t-Bu)3)2 + H2 oxidative addition. *J. Phys. Chem.* **100** (50), 19357–19363. https://doi.org/10.1021/jp962071j.
78. Felix Brandt and Christoph R. Jacob (2022). Systematic QM Region construction in QM/MM calculations based on uncertainty quantification. *J. Chem. Theory Comput.* **18** (4), 2584–2596. https://doi.org/10.1021/acs.jctc.1c01093.
79. A. Bilić, J. R. Reimers, and Hush.N.S. (2002). Adsorption of pyridine on the gold (111) surface: implications for "Alligator Clips" for molecular wires. *J. Phys. Chem. B* **106** (26), 6740–6747. https://doi.org/10.1021/jp020590i.
80. Walter Malone and Abdelkader Kara (2020). A coverage dependent study of the adsorption of pyridine on the (111) coinage metal surfaces. *Surface Science* **693**, 121525. https://doi.org/10.1016/j.susc.2019.121525.
81. M. Monajjemi, F. Mollaamin, M. R. Gholami, H. Yoosbashizadeh, S. K. Sadrnezhad, and H. Passdar (2003). Quantum chemical parameters of some organic corrosion inhibitors, Pyridine, 2-Picoline 4-Picoline and 2, 4- Lutidine, adsorption at aluminum surface in hydrocholoric and nitric acids and comparison between two acidic media. *Main Group Met. Chem.* **26**, 349–362.
82. Elodie Dumont, Charlotte De Bleye, Merzouk Haouchine, Laureen Coïc, Pierre-Yves. Sacré, Philippe Hubert, and Eric Ziemons (2020). Effect of the functionalisation agent on the surface-enhanced Raman scattering (SERS) spectrum: Case study of pyridine derivatives. *Spectrochimica Acta Part A: Mol. Biomol. Spectroscopy* **233**, 118180. https://doi.org/10.1016/j.saa.2020.118180.
83. Doreen Mollenhauer, Nicola Gaston, Elena Voloshina, and Beate Paulus (2013). Interaction of pyridine derivatives with a gold (111) Surface as a model for adsorption to large nanoparticles. *J. Phys. Chem. C* **117** (9), 4470–4479. https://doi.org/10.1021/jp309625h.
84. Cristina Isvoranu, Bin Wang, Evren Ataman, Karina Schulte, Jan Knudsen, Jesper N. Andersen, Marie-Laure. Bocquet, and Joachim Schnadt (2011). Pyridine adsorption on single-layer iron phthalocyanine on Au(111). *The J. Phys. Chem. C* **115** (41), 20201–20208. https://doi.org/10.1021/jp204460g.
85. A. D. Becke (1993). Density-functional thermochemistry. III. The role of exact exchange. *J. Chem. Phys.* **98**, 5648–5652.
86. C. Lee, W. Yang, and R. G. Parr (1988). Development of the Colle-Salvetti correlation-energy formula into a functional of the electron density. *Phys. Rev. B* **37**, 785–789.
87. K. Kim and K. D. Jordan (1994). Comparison of density functional and MP2 calculations on the water monomer and dimer. *J. Phys. Chem.* **98** (40), 10089–10094. https://doi.org/10.1021/j100091a024.
88. P. J. Stephens, F. J. Devlin, C. F. Chabalowski, and M. J. Frisch (1994). Ab Initio calculation of vibrational absorption and circular dichroism spectra using density functional force fields. *J. Phys. Chem.* **98** (45), 11623–11627. https://doi.org/10.1021/j100096a001.
89. C. J. Cramer (2004) Essentials of computational chemistry: theories and models, 2nd Edition | Wiley". Wiley.com. Retrieved 2021–06–24.
90. S. H. Vosko, L. Wilk, and M. Nusair (1980). Accurate spin-dependent electron liquid correlation energies for local spin density calculations: a critical analysis. *Can. J. Phys.* **58** (8), 1200–1211. https://doi.org/10.1139/p80-159.
91. Y. Xiao-Ci, Z. Hong, L. Ming-Dao, and R. Hong-Xuan (2000). *Lu-An, Y.* **42**, 645–653.